Hindawi
Advances in Materials Science and Engineering
Volume 2022, Article ID 6528470, 8 pages
https://doi.org/10.1155/2022/6528470

Research Article

The Effects of Minor Element Addition on the Structural Heterogeneity and Mechanical Properties of ZrCuAl Bulk Metallic Glasses

R. Sivaraman,[1] Indrajit Patra,[2] Zainab Mohsen Najm,[3] Noora M. Hameed,[4] Taif Alawsi,[5] and Seyedmasoud Hashemi[6]

[1]*Department of Mathematics, Dwaraka Doss Goverdhan Doss Vaishnav College, University of Madras, Chennai, India*
[2]*Ph.D from NIT Durgapur, West Bengal, India*
[3]*Anesthesia Techniques Department, Al-Mustaqbal University College, Babylon, Iraq*
[4]*Anesthesia Techniques Department, Al-Nisour University College, Baghdad, Iraq*
[5]*Scientific Research Center, Al-Ayen University, Thi-Qar, Iraq*
[6]*Department of Chemistry, Iran University of Science & Technology (IUST), Tehran, Iran*

Correspondence should be addressed to Seyedmasoud Hashemi; smhashemi33@gmail.com

Received 19 June 2022; Revised 15 July 2022; Accepted 27 July 2022; Published 27 August 2022

Academic Editor: Majid Samavatian

The present study reveals the role of Nb and Ni minor addition on the nanomechanical properties and nanostructure of ZrCuAl bulk metallic glass (BMG). For this purpose, atomic force microscopy (AFM) was used to evaluate the viscoelastic response of the BMG surface at the nanoscale, while the nanoindentation technique was applied to show the mechanism of plastic deformation. The results indicated that minor Nb addition decreased the relaxation of enthalpy accompanied by the weakening of structural heterogeneity. On the other hand, Ni addition improved the stored energy of the material and intensified the distribution of loosely packed regions in the microstructure. Moreover, the mechanical test unveiled that Ni addition enhanced the viscoelastic response; however, it came at the expense of creep resistance. The evaluation of the magnitude of the derivative in the nanoindentation test also demonstrated that the Ni-added sample exhibited a multiple shear-band mode for plastic deformation.

1. Introduction

Due to their amorphous structure, bulk metallic glasses (BMGs) possess excellent properties such as good corrosion resistance, superior strength, and sound magnetic features [1–5]. However, the inhomogeneous plastic deformation under the external loadings limits their applications in the industries [6, 7]. In recent years, minor element addition has been one of the main methods for improving the homogenous plastic deformation and strength in the BMGs [8–10]. The intensification of structural heterogeneity in the amorphous alloy determines the level of homogenous plasticity. The heterogeneity in the glassy structure has originated from the random scatter of loosely packed region free volumes in a rigid backbone with short and medium orders [11]. Considering the microalloying process, Zhu et al. [12] indicated that Sc addition into ZrCuNiAlTi BMG improved spatial heterogeneity and plastic deformation, which was due to the large atomic radius of Sc and the significant atomic size mismatch in the structure. Liang et al. [13] reported that an appropriate substitution of Fe by W enhanced both plastic deformation and ultimate compressive strength in the FeCrMoWCBY BMG. Teng et al. [14] revealed that the hydrogen microalloying process induced more liquid-like regions and abundant flow units, triggering the shear events and homogenous plastic deformation. It was also found that the hydrogen microalloying activated soft spots and improved structural heterogeneity, leading to the promotion of multiple shear bands [15]. Jin et al. [16] demonstrated that partial substitution of Hf with Cu

enhanced the compressive yield strength with a large plastic strain. Cao et al. [17] reported that minor element addition with positive heat of mixing into a ZrCuAl amorphous alloy not only improved the glass formation but also induced homogenous plastic deformation. Based on their results, the elements with smaller positive heat of mixing were more efficient in the improvement of glass formation owing to liquid stabilization, while elements with medium positive heat of mixing enhanced plastic deformation through the intensification of structural heterogeneity.

As aforementioned, proper minor addition may improve the structural heterogeneity and homogenous plastic deformation in the BMGs. Nevertheless, it is required to identify the microalloying effect on the structural heterogeneity with the high-resolution instruments. In recent years, atomic force microscopy (AFM) has been offered for this purpose [18–20]. For example, Mahmoud et al. [21] applied dynamic AFM to characterize the relaxation of nanoscale regions in a shock-peened BMG. Using high-resolution AFM, it was found that chemical variations changed the structural heterogeneity in the amorphous alloys [22]. Samavatian et al. [23] indicated that the low-dissipated regions resisted the energy alterations under repetitive AFM scanning, while high-dissipated regions exhibited a stochastic behavior. Using a contact resonance AFM, it was reported that the nanoscale zones with eminent heterogeneity induced a broad energy state distribution in the system [24]. The mentioned works clearly indicate that the AFM is an efficient instrument for the evaluation of nanoscale regions at the surface of BMGs. Hence, we used this method to characterize the nanoscale structural heterogeneity of BMGs under the minor addition. For this purpose, the $Zr_{57}Cu_{32}Al_{10}$ BMG was selected as the base alloy, while Ni and Nb elements were applied as the dopants. It is believed that the differences in the atomic size and thermodynamic behaviors of Ni and Nb significantly change the thermal behavior, microstructure, and mechanical properties in the ZrCuAl alloy. Hence, it is expected that the results shed light on the relation between the structural evolution, plastic deformation, and strength in this alloy.

2. Materials and Methods

For materials preparation, ingots with the alloying compositions of $Zr_{57}Cu_{32}Al_{10}$, $(Zr_{57}Cu_{32}Al_{10})_{97}Ni_3$, and $(Zr_{57}Cu_{32}Al_{10})_{97}Nb_3$ were fabricated through the arc melting of elements with >99.8% purity. Afterwards, the water-cooled copper mold casting was applied to produce BMG plates with dimensions of $10\,mm \times 10\,mm \times 3\,mm$. The differential scanning calorimetry (DSC) and X-ray diffraction (XRD) tests were also carried out to characterize the thermal features and amorphousness of BMG plates.

To study the structural heterogeneity, high-resolution atomic force microscopy (AFM) was applied in the tapping mode. In this experiment, the samples were cut from the plates and polished to obtain a uniform surface. A sharp probe with a tip diameter of $\sim 2\,nm$ facilitates the high-resolution scanning of samples. The energy dissipation of surfaces was calculated from the phase shift measurement [21]. To attain reliable results, AFM scanning was conducted in different windows on the sample surfaces. Considering (1), the energy dissipation of the surface can be calculated in accordance with the phase shift measurements [25]:

$$E_{\mathrm{dis}} = \left[\frac{\pi.K.A_{sp}.A_0.(\sin(\pi/2-\varphi))}{Q}\right] - \frac{A_{sp}}{A_0}. \quad (1)$$

In this equation, Q and K are the damping factor and the spring constant. The phase shift is defined by φ, while the set-point amplitude and free amplitude are shown by A_{sp} and A_0, respectively. The details for the calculation of energy dissipation are given in [25, 26]. The nanomechanical properties of BMG samples were also evaluated by the nanoindentation test. The experiment was conducted at room temperature under loading rates of $1\,\mathrm{mNs}^{-1}$. The holding time at maximum load was 10 s, whereas the maximum load was 25 mN. Thermal drift correction was also performed to remove drift effects and obtain accurate results with minimum fluctuations. To make the statistical evaluation possible, 80 indenting points were tested for each sample. Moreover, the magnitude of the derivative ($dh/dp^{0.5}$) was calculated for each state. In general, this term indicates the variations of pop-ins concerning the indenting load.

3. Results and Discussion

The XRD patterns of specimens are illustrated in Figure 1(a). The results indicated that there existed no sign of sharp Bragg peaks in the XRD patterns, meaning the absence of long-range orders in the atomic structure of samples. Figure 1(b) represents the thermal history of samples in the relaxation region. As observed, the enthalpy of relaxation is 7.7 J/g, 8.1 J/g, and 6.9 J/g in the ZrCuAl, ZrCuAlNi, and ZrCuAlNb samples, respectively. This outcome implies that Ni addition increases the stored energy in the system, leading to the intensification of structural heterogeneity, while Nb addition creates a relaxed structure with a more stable atomic configuration.

To characterize the structural heterogeneity, it is required to measure the distribution of energy dissipation in the amorphous alloys. One should note that the tapping load of the AFM tip is restricted so that no plastic deformation occurs on the surfaces. Hence, the energy dissipation of the surface is just a result of the viscoelastic response of the amorphous structure to the external excitation (tip tapping) [27]. Figure 2 shows the linear scanning of phase shift and topography analysis in the same position for the ZrCuAl sample. As can be seen, the phase shift and the height variation exhibit a different trend, meaning that there is no strong correlation between the phase lag and the roughness of the sample. Moreover, the height fluctuation at the surface is in the range of 0.2–0.75 nm, which indicates that careful polishing leads to a smooth surface. Figure 3 gives the 2D maps of energy dissipation for all the samples. As demonstrated, the high-dissipated-energy regions are embedded in a backbone with low dissipated energy. Generally, structural defects such as free volumes are the regions that dissipated

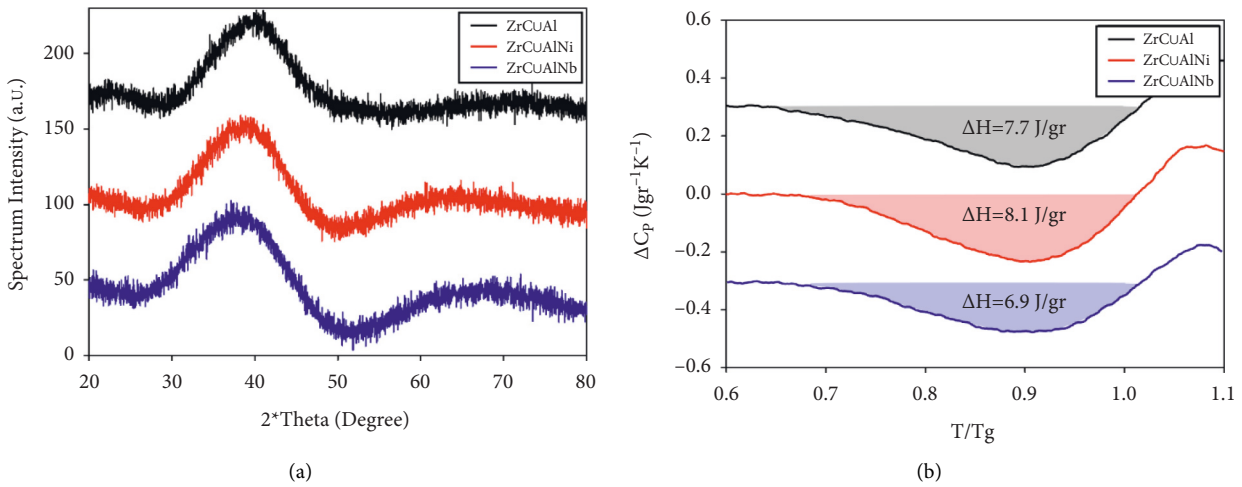

Figure 1: (a) XRD patterns and (b) DSC curves at the relaxation region for all the samples.

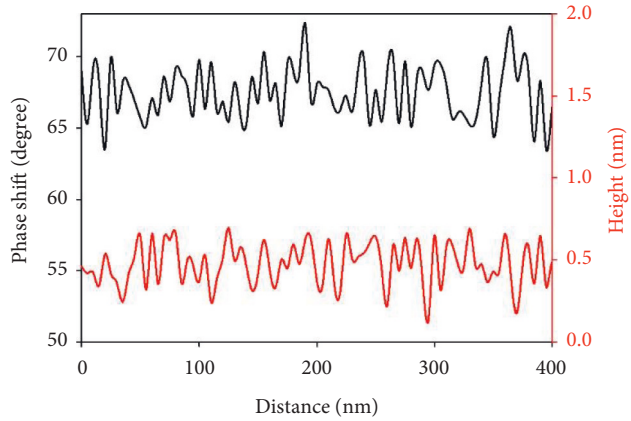

Figure 2: Linear scanning of phase shift and topography in the same position for ZrCuAl.

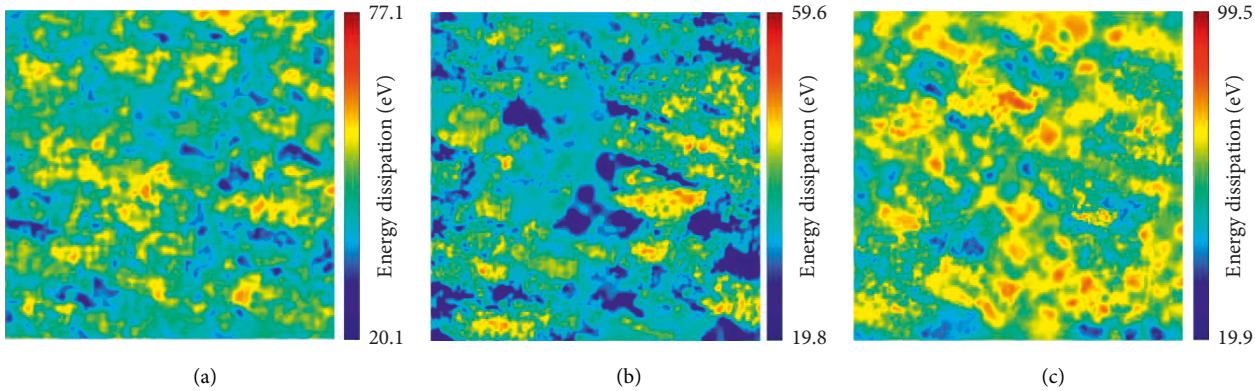

Figure 3: 2D maps of energy dissipation with a scanning size of 400×400 nm^2 for (a) ZrCuAl, (b) ZrCuAlNb, and (c) ZrCuAlNi.

energy significantly, while the short-range and medium-range orders are densely packed structures with low dissipated energy [18]. This event is due to the fact that the free volumes exhibit a viscoelastic response under tip tapping, leading to a huge energy release, while the dense regions show a rigid reaction such as crystalline alloys [28]. This description clearly indicates that why the metallic glasses have heterogeneous structures at the nanoscale. However, the results revealed that the intensification of heterogeneity is different in each sample. For the ZrCuAl alloy, the energy dissipation is in the range of 20.1–77.1 eV. On the other hand, ZrCuAlNi exhibits an energy dissipation range of

19.8–99.5 eV, showing the intensification of structural heterogeneity, whereas, the Nb-added sample shows a weak heterogeneity with a narrow range of energy dissipation values of 19.8–59.6 eV. As mentioned in Figure 1, the Nb-added sample included the minimum stored energy which is consistent with the weak structural heterogeneity. On the other hand, the Ni-added sample has a high enthalpy of relaxation, meaning that the system tends to show sharp heterogeneity in its structure. To conduct a detailed study, the FFT analysis of energy dissipation based on a polar presentation is given in Figure 4. According to the results, the data for the ZrCuAl alloy are distributed in an oval shape at the center of the figure. For ZrCuAlNi, the data distribution is more sporadic and has a sharp oval deviated configuration at the center. On the other hand, the collected data for the Nb-added sample are intensified at the center, implying the weak structural heterogeneity in this state. The Gaussian-type distribution of energy dissipation for the samples is represented in Figure 5(a)–5(c). As measured, the mean values of energy for ZrCuAl, ZrCuAlNb, and ZrCuAlNi are 40.2 eV, 48.3 eV, and 51.5 eV, respectively. The results also indicated that the ZrCuAlNb alloy has a sharp energy distribution, whereas the Ni-added sample exhibits a widened distribution which is also shifted to the higher energy values. To quantitatively analyze the structural heterogeneity in the samples, it is possible to determine the correlation function by using the length scale of loosely packed regions (ξ) in the atomic structure [29]:

$$P(r) = 2\sigma^2\left[1 - \exp\left(-\left(\frac{r}{\xi}\right)^{2\alpha}\right)\right], \quad (2)$$

where the α and σ parameters introduce the phase shift exponent and root mean square of phase shift values, respectively. Moreover, the correlation function can be defined through $P(r) = \langle P_1(r) - P(0)\rangle^2$, in which $P_1(r)$ and $P(0)$ are the phase shift values at the coordinate (x, y) and the reference position (0, 0), respectively [29]. Figure 5(d) shows the $P(r)$ curves as a function of distance. Data fitting of $P(r)$ makes possible the extraction of correlation lengths (ξ) for the samples. It is observed that Ni minor addition leads to the increase of correlation length from 6.41 nm (ZrCuAl) to 8.34 nm, while ZrCuAlNb experiences a low ξ value (5.91 nm). This result clarifies that the size of loosely packed regions significantly decreases with the addition of Nb into the base alloy. Other works also confirmed that Nb or Ni addition markedly changes the structural features of ZrCuAl amorphous alloys [30]. Moreover, it is suggested that minor Ni addition enhances the total negative enthalpy of mixing in the material and manifolds the types of short-range order (SRO) clusters but not their populations, leading to an increase of relaxation enthalpy. In this state, the rise in SRO types alters the medium-range orders (MROs) from the interpenetrated arrangements to the loose configurations, which provides potential sites for the nucleation of shear transformation zones (STZs) in the structure. On the other hand, the pair distribution function (PDF) analysis indicates that minor Nb addition leads to the shrinkage of SRO clusters, which is due to the strong interaction of Zr and Nb atoms accompanied by bond shortening in the system [31]. Furthermore, Nb addition densifies the spatial connections in the structure and intensifies the interpenetrated MROs in the ZrCuAlNb alloy. This phenomenon is due to the decrease of Zr-centered and Al-centered clusters that are responsible for the creation of nanoscale loose regions in the ZrCuAl BMG [30]. Hence, it is concluded that Nb addition increases the dense atomic orders and decreases the enthalpy of relaxation and structural heterogeneity in the ZrCuAl BMG.

The load-displacement curves of BMG specimens are represented in Figure 6(a). It is found that Ni addition significantly enhances the displacement (h) of BMG; however, Nb addition leads to the decrease of plastic deformation under the nanoindentation process. Moreover, Ni addition intensifies creep displacement at the maximum load. This means that the Ni-added sample is exposed to higher plastic deformation under constant loading, which is due to the increase of potential sites for the creation and generation of nanoscale shear events during the indenting process. To make a detailed comparison, the maximum indentation depth (d_{max}) and the final indentation depth (d_f) in the curves are evaluated. As given in Figure 6(b), the d_f/d_{max} ratio in the ZrCuAlNi alloy is higher than other samples. High d_f/d_{max} means that the BMG sample stores significant anelastic energy in its microstructure. In general, the creep event in the amorphous alloys includes the viscoelastic and viscoplastic strains. Based on our results, the Ni-added sample shows a great viscoelastic response to external excitation (higher d_f/d_{max}), which is due to the intensified structural heterogeneity; however, this sample experiences a huge viscoplastic strain at the maximum load, showing that it is a sign of severe creep deformation. On the other hand, the Nb-added sample shows a reverse behavior compared to the ZrCuAlNi BMG, which implies that Nb addition improves the creep resistance through the prevention of nanoscale strain localization in its atomic structure. In order to evaluate the variations of strength and mechanical properties, it is necessary to conduct a statistical analysis regarding the hardness and Young's modulus of BMGs. Figure 7 indicates the correlation between the hardness/elastic modulus of samples and the displacement at the maximum load (creep displacement). The results clearly unveil that Ni addition leads to the decrement of hardness and Young's modulus so that the mean values of hardness and Young's modulus for ZrCuAlNi are 13% and 19% lower than the ZrCuAl alloy, respectively. On the other side, the Nb-added sample exhibits higher hardness and Young's modulus values compared to the base alloy. Furthermore, one can see that the distribution of Young's modulus and hardness shows a linear trend with statistical Pearson correlation coefficients of −0.892 and −0.855 and the negative slopes of −2.13 and $-0.94\,\mathrm{nm\,GPa^{-1}}$, respectively. The similarities in the trends of properties indicate that minor addition simultaneously affects Young's modulus and hardness; however, one can see that the elastic modulus is more sensitive to the microalloying process. The results also reveal that the distribution of data in the Ni-added sample is more sporadic compared to the other samples. This outcome

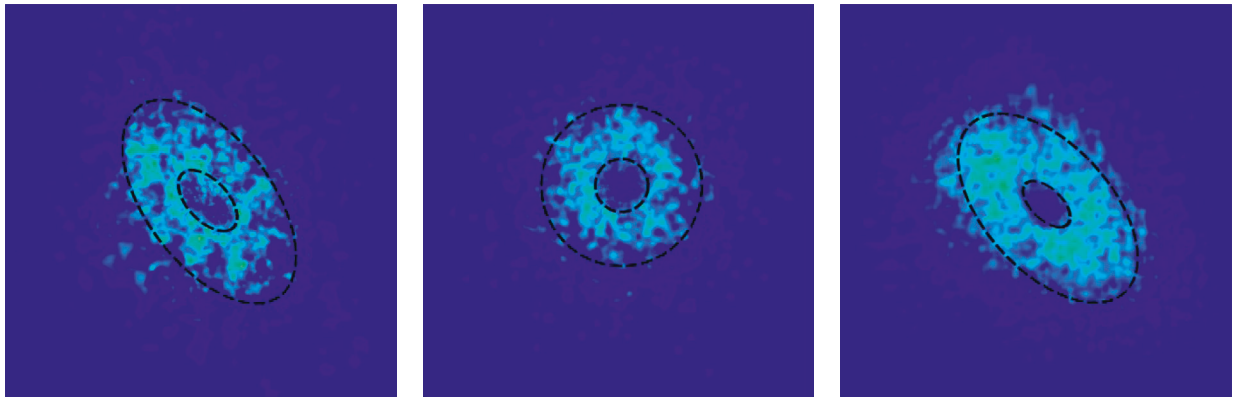

Figure 4: FFT data for energy dissipation in (a) ZrCuAl, (b) ZrCuAlNb, and (c) ZrCuAlNi.

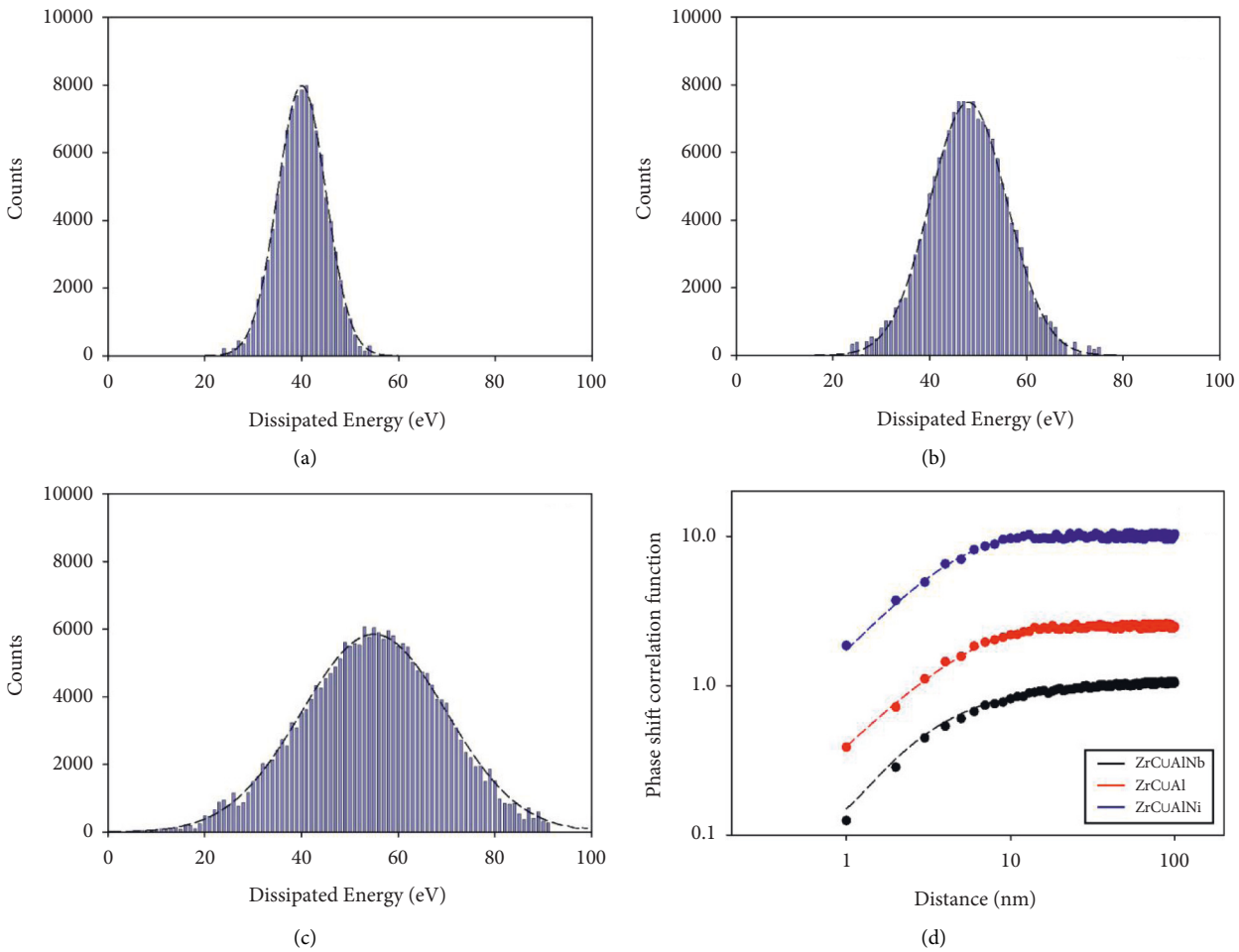

Figure 5: Gaussian energy distribution for (a) ZrCuAl, (b) ZrCuAlNb, (c) ZrCuAlNi, and (d) phase shift correlation function for all the samples.

suggests that the increase of structural heterogeneity is accompanied by the diversity of nanoscale regions with various local mechanical properties, leading to sporadic data distribution.

Figure 8 provides information regarding the correlation between the pop-in displacements and the load/magnitude of the derivative. The results indicate that the low magnitude of derivatives is associated with the small pop-in events. Moreover, it is found that Ni addition leads to shrinkage of data in the plots, meaning that the mechanism of plastic deformation in the Ni-added sample is consistent with the creation and propagation of multiple small shear events in

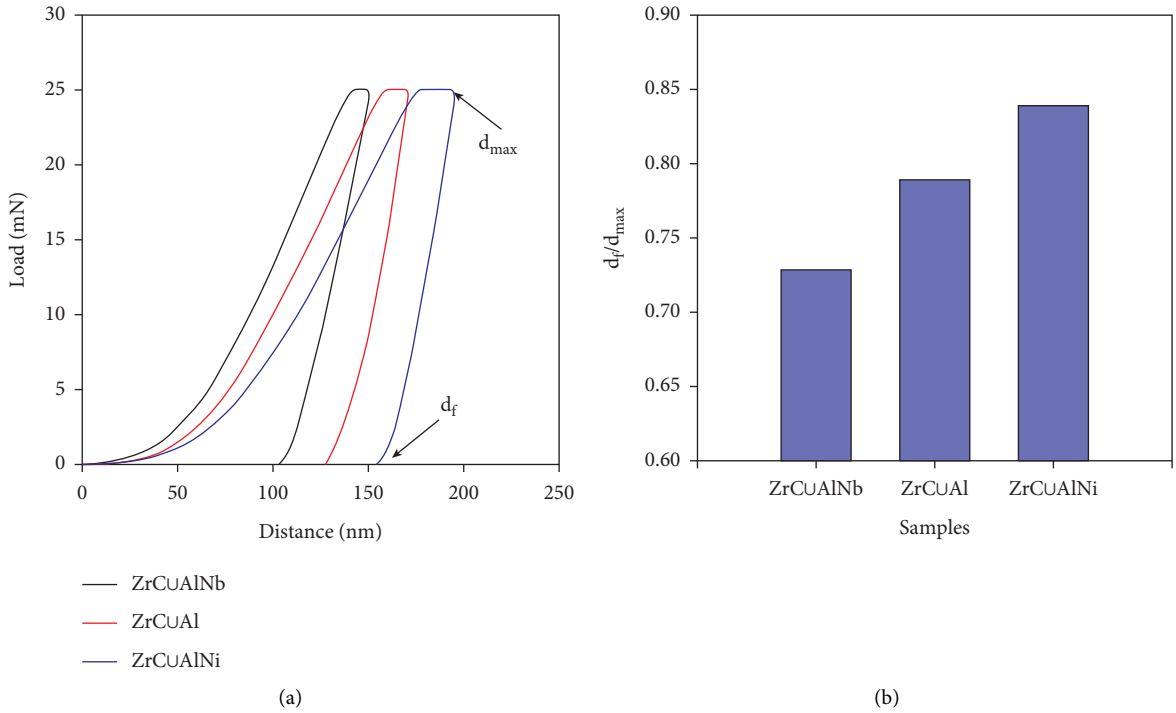

Figure 6: (a) Load-displacement curve and (b) d_f/d_{max} ratio for all the samples.

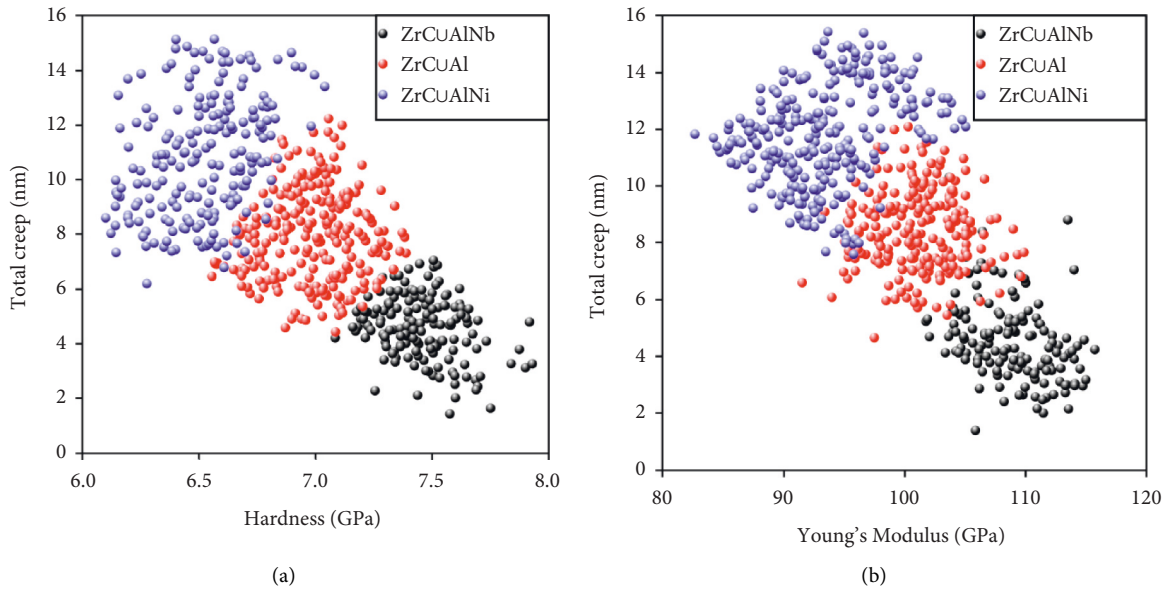

Figure 7: Total creep displacement as a function of (a) hardness and (b) Young's modulus.

the microstructure. On the other hand, the Nb-added sample exhibits the highest sporadic data in the plots, which implies the formation of main shear bands with highly localized strains. In other words, the Ni-added sample with the highest enthalpy of relaxation contains a huge amount of free volumes in its amorphous structure. In this state, the structural heterogeneity is more pronounced in the system, leading to the intensification of stress fields in the nanoscale regions. Hereupon, numerous shear events are formed and generated when an external loading is applied to the material. On the other hand, the high magnitude of the derivative in the Nb-added sample indicates that the shear bands can easily propagate through the sample without any interactions with other shear bands.

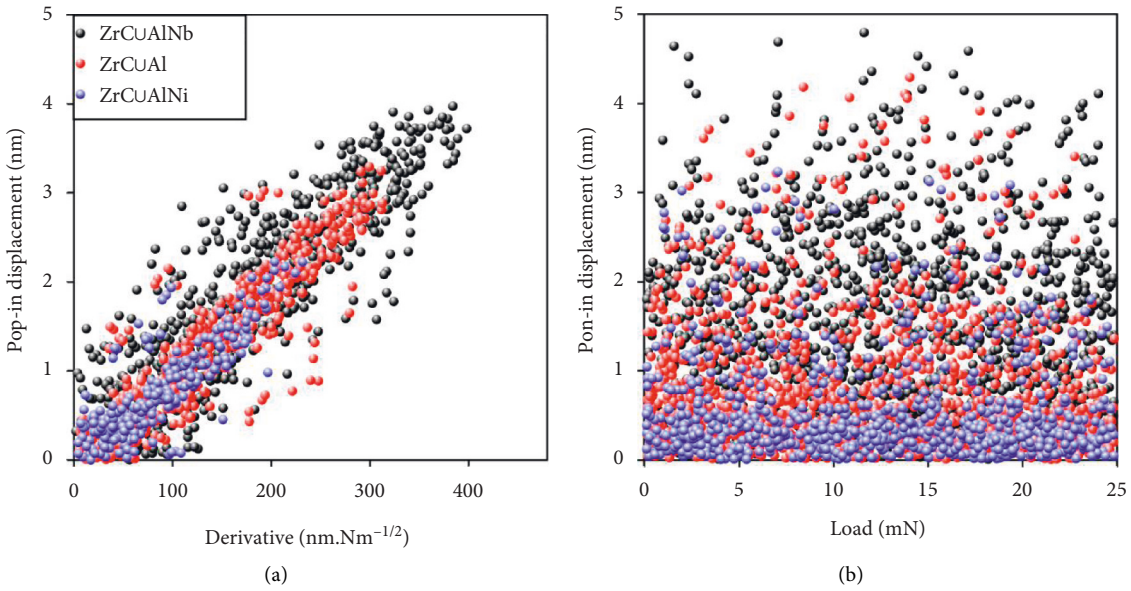

Figure 8: Pop-in displacement variations as a function of (a) load derivative and (b) load value.

4. Conclusions

The outcome of this work indicates how the minor addition of Ni and Nb elements can tune the structural features and nanomechanical properties of the ZrCuAl BMG. Based on the results, it is found that the Ni element is a promising constitute for increasing the total negative heat of mixing in the ZrCuAl system, leading to the improvement of relaxation enthalpy and structural heterogeneity. On the other hand, the Nb element shows a strong interaction with zirconium, which intensifies the SRO and MRO structures and reduces the fluctuations of structural variations in the amorphous alloy. The nanoindentation test also showed that the Nb-added sample has a lower displacement at the maximum load, which is a proper state for creep applications, whereas, the Ni-added sample exhibits a strong viscoelastic response, meaning that Ni addition is responsible for the creation and distribution of more loosely packed regions in the atomic structure.

Data Availability

The [DATA TYPE] data used to support the findings of this study are included within the article.

Conflicts of Interest

The authors declare that they have no conflicts of interest.

References

[1] X. S. Wei, J. L. Jin, Z. Z. Jiang, D. D. Liang, and J. Shen, "FeCrMoWCBY metallic glass with high corrosion resistance in molten lead–bismuth eutectic alloy," *Corrosion Science*, vol. 190, Article ID 109688, 2021.

[2] N. Sohrabi, J. Jhabvala, G. Kurtuldu et al., "Characterization, mechanical properties and dimensional accuracy of a Zr-based bulk metallic glass manufactured via laser powder-bed fusion," *Materials & Design*, vol. 199, Article ID 109400, 2021.

[3] N. Sohrabi, M. Hamidi-Nasab, B. Rouxel et al., "Fatigue performance of an additively manufactured Zr-based bulk metallic glass and the effect of post-processing," *Metals*, vol. 11, no. 7, p. 1064, 2021.

[4] P. Zhang, C. Zhang, and L. Liu, "Toughening 3D-printed Zr-based bulk metallic glass via synergistic defects engineering," *Materials Research Letters*, vol. 10, no. 6, pp. 377–384, 2022.

[5] S.-X. Liang, S. Salamon, S. Zerebecki et al., "A laser-based synthesis route for magnetic metallic glass nanoparticles," *Scripta Materialia*, vol. 203, Article ID 114094, 2021.

[6] W. Zhou, Y. Meng, F. Duan et al., "The effect of oxygen on phase formation in an industrial Zr based bulk metallic glass," *Intermetallics*, vol. 129, Article ID 107055, 2021.

[7] F. Xie, Q. Chen, and J. Gao, "Brittle-ductile transition in laser 3D printing of Fe-based bulk metallic glass composites," *Metals*, vol. 9, no. 1, p. 78, 2019.

[8] Y. J. Yang, B. Y. Cheng, J. W. Lv et al., "Effect of Ag substitution for Ti on glass-forming ability, thermal stability and mechanical properties of Zr-based bulk metallic glasses," *Materials Science and Engineering A*, vol. 746, pp. 229–238, 2019.

[9] Z. Long, P. Tao, G. Wang et al., "Effect of Nb and Ta addition on mechanical properties of Zr-based bulk metallic glasses and composites," *Journal of Alloys and Compounds*, vol. 912, Article ID 165071, 2022.

[10] T. Wang, Q. Hou, and L. Zhang, "Enhanced heterogeneity and plasticity in a Zr-Cu–Al bulk metallic glass with micro-addition of oxygen," *Materials Science and Engineering A*, vol. 831, Article ID 142222, 2022.

[11] H. B. Ke, J. F. Zeng, C. T. Liu, and Y. Yang, "Structure heterogeneity in metallic glass: modeling and experiment," *Journal of Materials Science & Technology*, vol. 30, no. 6, pp. 560–565, 2014.

[12] J. Zhu, W. Gao, S. Cheng et al., "Improving the glass forming ability and plasticity of ZrCuNiAlTi metallic glass by substituting Zr with Sc," *Journal of Alloys and Compounds*, vol. 909, Article ID 164679, 2022.

[13] D. D. Liang, X. S. Wei, C. T. Chang, J. W. Li, X. M. Wang, and J. Shen, "Effect of W addition on the glass forming ability and mechanical properties of Fe-based metallic glass," *Journal of Alloys and Compounds*, vol. 731, pp. 1146–1150, 2018.

[14] Y. Teng, Y. Song, S. J. Xie, and Z. D. Sha, "On the deformation and failure mechanisms of hydrogen alloyed metallic glasses," *Journal of Applied Physics*, vol. 131, no. 8, Article ID 085104, 2022.

[15] L. S. Luo, B. B. Wang, F. Y. Dong et al., "Structural origins for the generation of strength, ductility and toughness in bulk-metallic glasses using hydrogen microalloying," *Acta Materialia*, vol. 171, pp. 216–230, 2019.

[16] Z. S. Jin, Y. J. Yang, Z. P. Zhang et al., "Effect of Hf substitution Cu on glass-forming ability, mechanical properties and corrosion resistance of Ni-free Zr–Ti–Cu–Al bulk metallic glasses," *Journal of Alloys and Compounds*, vol. 806, pp. 668–675, 2019.

[17] D. Cao, Y. Wu, X. J. Liu, H. Wang, X. Z. Wang, and Z. P. Lu, "Enhancement of glass-forming ability and plasticity via alloying the elements having positive heat of mixing with Cu in Cu48Zr48Al4 bulk metallic glass," *Journal of Alloys and Compounds*, vol. 777, pp. 382–391, 2019.

[18] M. Gao and J. H. Perepezko, "Mapping the viscoelastic heterogeneity at the nanoscale in metallic glasses by static force spectroscopy," *Nano Letters*, vol. 20, no. 10, pp. 7558–7565, 2020.

[19] C. Ebner, B. Escher, C. Gammer, J. Eckert, S. Pauly, and C. Rentenberger, "Structural and mechanical characterization of heterogeneities in a CuZr-based bulk metallic glass processed by high pressure torsion," *Acta Materialia*, vol. 160, pp. 147–157, 2018.

[20] F. Zhu, S. Song, K. M. Reddy, A. Hirata, and M. Chen, "Spatial heterogeneity as the structure feature for structure–property relationship of metallic glasses," *Nature Communications*, vol. 9, pp. 3965–3967, 2018.

[21] Z. H. Mahmoud, H. Barazandeh, S. M. Mostafavi et al., "Identification of rejuvenation and relaxation regions in a Zr-based metallic glass induced by laser shock peening," *Journal of Materials Research and Technology*, vol. 11, pp. 2015–2020, 2021.

[22] N. Wang, J. Ding, P. Luo, Y. Liu, L. Li, and F. Yan, "Chemical variation induced nanoscale spatial heterogeneity in metallic glasses," *Materials Research Letters*, vol. 6, no. 12, pp. 655–661, 2018.

[23] M. Samavatian, R. Gholamipour, D. O. Bokov, W. Suksatan, V. Samavatian, and M. Mahmoodan, "Characterization of nanoscale structural heterogeneity in metallic glasses: a machine learning study," *Journal of Non-crystalline Solids*, vol. 578, Article ID 121344, 2022.

[24] D. P. Wang, J. C. Qiao, and C. T. Liu, "Relating structural heterogeneity to β relaxation processes in metallic glasses," *Materials Research Letters*, vol. 7, no. 8, pp. 305–311, 2019.

[25] M. Samavatian, R. Gholamipour, A. A. Amadeh, and V. Samavatian, "Inherent relation between atomic-level stresses and nanoscale heterogeneity in Zr-based bulk metallic glass under a rejuvenation process," *Physica B: Condensed Matter*, vol. 595, Article ID 412390, 2020.

[26] F. Zhu, H. K. Nguyen, S. X. Song et al., "Intrinsic correlation between β-relaxation and spatial heterogeneity in a metallic glass," *Nature Communications*, vol. 7, no. 1, p. 11516, 2016.

[27] Y. M. Lu, J. F. Zeng, S. Wang et al., "Structural signature of plasticity unveiled by nano-scale viscoelastic contact in a metallic glass," *Scientific Reports*, vol. 6, no. 1, Article ID 29357, 2016.

[28] S. Ouyang, L. J. Song, Y. H. Liu et al., "Correlation between the viscoelastic heterogeneity and the domain wall motion of Fe-based metallic glass," *Physical Review Materials*, vol. 2, no. 6, Article ID 063601, 2018.

[29] Z. Z. Yang, L. Zhu, L. X. Ye et al., "Nanoscale structural heterogeneity perspective on the improved magnetic properties during relaxation in a Fe-based metallic glass," *Journal of Non-crystalline Solids*, vol. 571, Article ID 121078, 2021.

[30] Q. H. Pham, S. Chupradit, G. Widjaja et al., "The effects of Ni or Nb additions on the relaxation behavior of Zr55Cu35Al10 metallic glass," *Materials Today Communications*, vol. 29, Article ID 102909, 2021.

[31] S. Y. Wu, S. H. Wei, G. Q. Guo, J. G. Wang, and L. Yang, "Structural mechanism of the enhanced glass-forming ability in multicomponent alloys with positive heat of mixing," *Scientific Reports*, vol. 6, no. 1, Article ID 38098, 2016.